Comparison of branching ratio and sum-rule analyses of magnetic circular dichroism in x-ray-absorption spectroscopy

J. G. Tobin
Department of Chemistry and Materials Science, Lawrence Livermore National Laboratory, Livermore, California 94550

G. D. Waddill
Department of Physics, University of Missouri–Rolla, Rolla, Missouri 65401-0249

A. F. Jankowski
Department of Chemistry and Materials Science, Lawrence Livermore National Laboratory, Livermore, California 94550

P. A. Sterne
Department of Chemistry and Materials Science, Lawrence Livermore National Laboratory, Livermore, California 94550 and Department of Physics, University of California, Davis, Davis, California 95616

D. P. Pappas
Department of Physics, Virginia Commonwealth University, Richmond, Virginia 23284-2000
(Received 16 November 1994; revised manuscript received 2 February 1995)

Two localized picture methods of analyzing the magnetic circular dichroism in x-ray absorption will be applied to experimental results: the branching ratio (BR) and sum rule (SR) approaches. A derivation of the BR formulas and detailed comparison to the SR expressions will be made, including error estimations. The BR approach will be seen to be a limiting case form of the SR spin-moment expression and provide a simple picture of the underlying physics in magnetic x-ray circular dichroism absorption in 3*d* magnetic materials.

I. INTRODUCTION

In the past several years there has been a surge of interest in using circularly-polarized x rays as a probe of electronic and magnetic structure in magnetic material systems.[1–8] One particularly simple, yet powerful, measurement is x-ray absorption,[1–6] where strong variations can be induced by changing the helicity or circular polarization of the x rays. In this experiment, an x ray is absorbed, promoting an electron from a core level into an empty, unoccupied state (Fig. 1). The strong variations occur in the peak or "white line" structure at the edge jumps (Fig. 2). In this work, attention will be focused almost exclusively upon *p* to *d* transitions in 3*d* magnetic materials. These peaks occur at the absorption thresholds because of the large density of unoccupied *d* states immediately above the Fermi energy. In magnetic systems, this is split into majority and minority density of states. The transitions are electric dipole in nature and exhibit a strong dependence upon the relative alignments of the magnetization vector and helicity, which will be defined below.

In the pioneering work of Shütz *et al.*[1] and Chen *et al.*[2] fairly small effects were observed and results were reported in terms of asymmetries. The asymmetry is defined as shown in Eq. (1) below:

$$\mathrm{asym}(h\nu)=\frac{i^{+}(h\nu)-i^{-}(h\nu)}{i^{+}(h\nu)+i^{-}(h\nu)} . \tag{1}$$

Here, the *i*'s are the intensities at a given photon energy ($h\nu$) and for each circular polarization configuration, parallel (+), and antiparallel (−). This refers to the relative orientation of the magnetization vector and the x-ray helicity. A lowercase *i* is used to indicate that peak intensities are *not* integrated in this approach. This method has the advantage of emphasizing small variations but requires very good statistics because of the difference taken

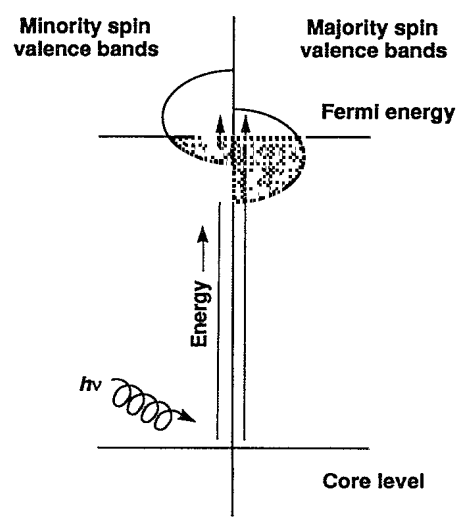

FIG. 1. Shown here is a schematic of the absorption of a photon and transition of an electron into an exchange split valence band density of states.

 ©1995 The American Physical Society

in the numerator and the absence of peak integration. Generally it is desirable to use a pair of edges with a sizable spin-orbit splitting and observe the relative change at each edge. An example is shown in Fig. 3. Alternatively, one can couch the changes in the spectra in terms of integrated peak areas.[4,9–13]

The use of the integrated peak areas has the following advantage: while the peak shapes tend to reflect details of the excited final state, the integrated areas correlate with the original ground state.[14–16] One approach to interpretation of integrated intensities is the use of branching ratios.[4,11–13] For the $2p$ peaks, the branching ratio (BR) is equal to the integrated intensity in the $2p_{3/2}$ divided by the sum of integrated intensities of the $2p_{3/2}$ and $2p_{1/2}$ peaks,

$$\mathrm{BR}=\frac{I(2p^{3/2})}{I(2p^{3/2})+I(2p^{1/2})} . \tag{2}$$

For the case shown in the upper panel of Fig. 2, the following expression would apply:

$$\mathrm{BR}^{+}=\frac{A^{+}}{A^{+}+B^{+}} . \tag{3}$$

Similarly, an expression for BR^{-} in terms of A^{-} and B^{-} also exists. This illustrates a salient feature of a BR analysis: the BR is fairly independent of the background determination (C^{+} or C^{-}) and does not require an interspectral normalization (C^{+} versus C^{-}), instead depending upon an intraspectral normalization.

Within a localized, one-electron picture of x-ray absorption,[17] particularly elegant expressions can be obtained for the branching ratio in certain simplified cases,

$$\mathrm{BR}^{d}=\frac{2}{3}-\frac{\vec{P}_{h\nu}\cdot\vec{P}_{e}}{6} \quad \text{for } 3d \text{ elements,} \tag{4}$$

$$\mathrm{BR}^{f}=\frac{6}{10}-\frac{\vec{P}_{h\nu}\cdot\vec{P}_{e}}{5}$$

$$\text{for } 4f \text{ and } 5f \text{ elements with } L\approx 0 . \tag{5}$$

Here, $\mathbf{P}_{h\nu}$ is the circular polarization of the photon and $\mathbf{P}_{e}$ is the polarization of the d (or f) valence band. These relations were introduced and used previously[4,12,13] to interpret magnetic x-ray circular dichroism (MXCD) absorption spectra in systems in which the orbital contribution was small[18] and the total magnetic moment was essentially the spin moment. A derivation of Eq. (4) is included in Appendix A, with definitions of the various expressions and their relation to previously used expressions. A failing of this simple picture is the absence of nonstatistical values for linear polarization $P_{h\nu}=0$.[6,11,19] However, much of this problem can be circumvented by inverting Eq. (4) and equating the spin magnetic moment ($\mu_{\mathrm{spin}}^{\mathrm{BR}}$) with an asymmetry of branching ratios (see Ap-

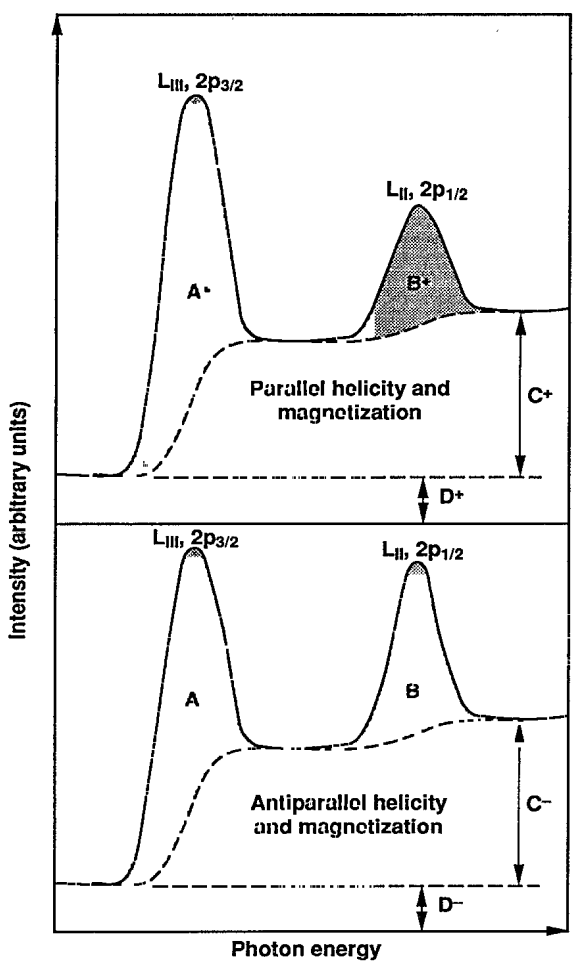

FIG. 2. Schematic of x-ray-absorption spectra with white line peaks at the L_{III} and L_{II} edges. This is for the case of ferromagnetic alignment. This is an idealized cartoon showing the essential quantities used in branching ratio and sum-rule analysis. Experimental spectra are much more complex, including noise, varying backgrounds, and other sources of limitation to information extraction.

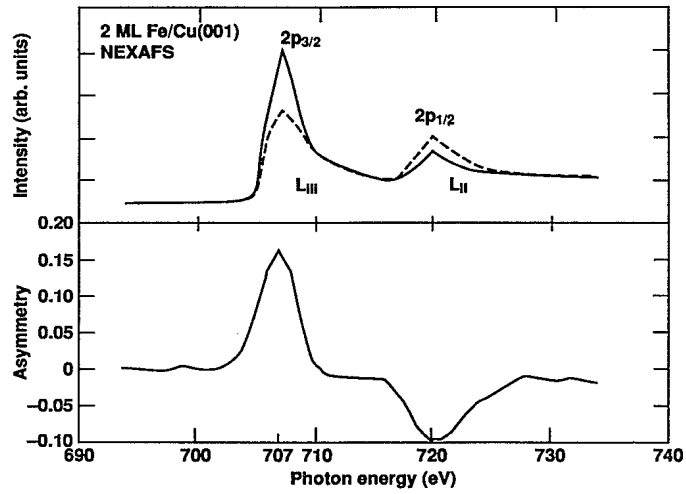

FIG. 3. In the upper panel are near-edge x-ray-absorption fine-structure (NEXAFS) spectra of 2 ML of Fe/Cu(001). The helicity is parallel (line) or antiparallel with the remanent magnetization vector, which is perpendicular to the surface at this coverage. The lower panel contains an asymmetry curve, calculated from the experimental spectra following Eq. (1).

pendix A). This permits us to focus on the key element, the variation of the branching ratio with polarization,

$$\mu_{\text{spin}}^{\text{BR}}=\frac{4(N)}{|P_{h\nu}|}\left[\frac{\text{BR}^{+}-\text{BR}^{-}}{\text{BR}^{+}+\text{BR}^{-}}\right] \quad \text{for } 3d \text{ elements.} \tag{6}$$

Here, n is the number of $3d$ valence electrons, $N=10-n$ is the number of $3d$ valence holes, and BR^{+} and BR^{-} are as described above [see Eq. (3)]. A pleasing aspect of this expression is its explicit retention of a dependence upon polarization, a significant concern for an experimentalist. While other experimental studies have used an *ad hoc* linear correction for polarization, this work provides a theoretical justification for such a correction in spin-moment measurements and demonstrates that the proper approach is via a branching-ratio-related method, not necessarily an intensity symmetry as in Eq. (1).

A far more sophisticated derivation, still within a localized, one-electron framework, has arrived at sum rules (SR) for the spin[10] and orbital[9] magnetic moments. For $3d$ elements and $2p\rightarrow 3d$ transitions these are summarized below in relation to the quantities defined in Fig. 2,

$$\mu_{\text{spin}}^{\text{SR}}=2\langle S_z\rangle=\frac{6(N)\left[\frac{A^{+}}{C^{+}}-\frac{A^{-}}{C^{-}}\right]}{\left[\frac{A^{+}}{C^{+}}+\frac{B^{+}}{C^{+}}+\frac{A^{-}}{C^{-}}+\frac{B^{-}}{C^{-}}\right]}-3\langle L_z\rangle-7\langle T_z\rangle\ , \tag{7}$$

$$\mu_{\text{orb}}^{\text{SR}}=\langle L_z\rangle=\frac{4}{3}(N)\frac{\left[\left[\frac{A^{+}}{C^{+}}+\frac{B^{+}}{C^{+}}\right]-\left[\frac{A^{-}}{C^{-}}+\frac{B^{-}}{C^{-}}\right]\right]}{\left[\frac{A^{+}}{C^{+}}+\frac{B^{+}}{C^{+}}+\frac{A^{-}}{C^{-}}+\frac{B^{-}}{C^{-}}\right]}. \tag{8}$$

A significant amount of debate remains concerning the general applicability of these rules[5,6,20–22] (i.e., the accuracy of their predictions versus the true result). For example, the magnetic dipole term $\langle T_z\rangle$ can be of importance in noncentrosymmetric systems, e.g., with surfaces and interfaces.[21] Dispersive and many-body effects also remain items of concern.[6] [Note also that the sum rules have been derived for the $P_{h\nu}=\pm 1$ ideal case. Again, a justified method of correction for nonideal polarization is required.]

A comparison of BR and SR approaches yields several interesting observations. (1) If $|\langle T_z\rangle|\ll|\langle S_z\rangle|$, then the $\mu_{\text{spin}}^{\text{SR}}$ and $\mu_{\text{spin}}^{\text{BR}}$ expressions are very closely related. In Appendix B, the following equation is derived:

$$\mu_{\text{spin}}^{\text{SR}}-\mu_{\text{spin}}^{\text{BR}}=(1-x)(\mu_{\text{spin}}^{\text{SR}}+3\mu_{\text{orb}}^{\text{SR}})\overset{\text{for Fe}}{\leq}0.2\mu_{\text{spin}}^{\text{SR}}\ . \tag{9}$$

In this case $X\approx(4/3)/(\text{BR}^{+}+\text{BR}^{-})$, a measure of the deviation from statistically (statisticality: $\text{BR}^{+}+\text{BR}^{-}=4/3$, and $\text{BR}^{\text{lin}}=2/3$). Thus, as one might expect, for the BR approach to hold, the departure from statisticality must be small and the orbital moment must be small relative to the spin moment.[18] (2) The branching ratio is handicapped in terms of measuring the orbital moment. Earlier work[11] indicated that the deviation of the branching ratio, obtained with linear polarization, from the statistical value of 2/3 was a measure of the valence band spin-orbit splitting. Nevertheless, the absence of any direct comparison of $(A^{+}+B^{+})$ versus $(A^{-}+B^{-})$ limits its measurement of μ_{orb}.

Thus, while the BR analysis will give us no measure of μ_{orb}, it may provide a fair estimate of μ_{spin}, and thus μ_{total}, in systems in which $|\mu_{\text{orb}}|\ll|\mu_{\text{spin}}|$. In $3d$ magnetic materials,[18] it is often the case that orbital quenching[23] is strong and hence the BR approach may be useable. Below we will test this hypothesis and the above relations with experimental results.

II. EXPERIMENT

The experiments were performed at the Standard Synchrotron Radiation Laboratory (SSRL) using the spherical grating monochromator of beam line 8-2, which is part of the facilities of the University of California/National Laboratories Participating Research Team (UC/NL-PRT).[24,25] This is a bending magnet beam line, where the circular polarization of the x-rays is obtained by moving the first mirror or an aperture so that the x rays above or below the horizontal plane are selectively accepted. For the Fe/Cu(001) samples, the absorption process was monitored in a "partial yield" mode, typically by counting electrons in a window near kinetic energy (KE) of 47 eV, thus emphasizing the contribution from the *MVV* Fe Auger electrons.[4] The spectrometer has been previously described.[26] The near-edge x-ray-absorption fine-structure (NEXAFS) measurements were normalized to photon flux via dividing by the output of an upstream I_0 detector, based upon a 95% transmitting grid of gold. The films were magnetized using a magnetic pulse of 3 kOe.[4,8] Fe/Cu(001) sample preparation, including cleaning and Fe evaporation, is described elsewhere.[27] We conservatively project a factor of 2 uncertainty in all absolute coverage estimates of the Fe overlayers, which does not strongly impact the results of the MXCD study. Base pressure was 2×10^{-10} Torr. In the case of the multilayer Fe/Pt samples, x-ray absorption was performed by partial and total yield measurements. Sample preparation of the Fe/Pt films was described previously.[12] Generally, NEXAFS measurements were made by aligning the sample magnetization and the Poynting vector of the x rays. For perpendicularly-magnetized samples this implies normal incidence, and in-plane magnetization requires grazing incidence (approximately within 10° of the surface plane). The relationships between the helicity vector and magnetization were varied by changing helicities, flipping magnetizations, and in the case of grazing incidence, moving the samples. All measurements were made in remanence. In our fits, an entire spectrum is fitted with two peak functions, two step functions, and a linear background with each edge having both a peak and step function. The integrated area of a function is used as the integrated intensity. This emphasizes the white-line characteristics and

tends to omit contributions from transitions into states other than the empty valence band d levels, e.g., s and p states.

III. ERROR ANALYSIS

A proper comparison of the sum rule and branching ratio results must include not only an evaluation of the deviation of $\mu_{\rm spin}^{\rm SR}$ versus $\mu_{\rm spin}^{\rm BR}$, but also realistic estimates of the errors propagated in each analysis. For example, consider Eqs. (6)–(8). First, lets look at a best case scenario. Neglecting the $\langle L_z \rangle$ and $\langle T_z \rangle$ terms in Eq. (7), each of the magnetic moment results, $\mu_{\rm spin}^{\rm SR}$, $\mu_{\rm spin}^{\rm BR}$, and $\mu_{\rm orb}^{\rm SR}$ is a fractional difference times a prefactor. Assuming that the polarization is 100%, the coefficient would be 4, 6, and 4/3 times (N), respectively. Using $N=4$ for Fe, $N=3$ for Cu, and $N=2$ for Ni, it is found that the prefactor is about 4 for $\mu_{\rm orb}$ and about 20 for $\mu_{\rm spin}$. Thus an uncertainty in any of the fractional differences of $\frac{1}{2}$% would give rise to errors of about $0.02\mu_B$ in the $\mu_{\rm orb}$ and about $0.1\mu_B$ in $\mu_{\rm spin}$. (This is essentially an issue of precision or reproducibility, with appropriate error propagation. We are not yet addressing accuracy, the issue of obtaining the true value.) A more complete summary is shown in Table I. Here it is assumed that N is known absolutely and the only error is from the area estimates. If an estimate of $\Delta N/N$ of 10% is applied, all of the values in Table I approximately *double*. Thus the values in Table I are probably the minimum error that can be reasonably expected.

These errors will appear regardless of whether one performs peak fitting[4] or spectral matching.[5,28,29] In peak fitting, analytic functions are used to simulate the spectra. In our case, two peak functions, two step functions, and a background were used. This approach has the advantage of focusing on the white line intensities with the removal of the underlying steps, typically associated with the sp density of unoccupied states and possible inelastic multi-electronic effects. The concomitant disadvantage is that there tend to be too many variable parameters for the data: restrictions of parameter space can lower error estimates and improve convergence of the fit, at the risk of introducing systematic errors. For example, variation of the height, position, and width of each step function can have a strong effect. Peak widths and positions can vary with resolution. Overlap of the two peak and two-step functions can cause uncertainty. Often times, it is difficult to obtain the proper peak shape. Alteratively, spectral matching allows the circumvention of some of these problems. As suggested by Eq. (1) and Figs. 2 and 3, one matches the pre-edge and post-edge regimes autoregressively,[28] i.e., set $D^+=D^-$ and $C^+=C^-$. A difference can then be taken between the two spectra, independent of any peak fitting. At this point, the difficulties begin, as it is necessary to arrive at meaningful estimates of

$$\left[\frac{A^+}{C^+}-\frac{A^-}{C^-}\right],\ \left[\frac{B^+}{C^+}-\frac{B^-}{C^-}\right],\ \text{etc}\ .$$

One option is to arbitrarily integrate above and below zero intensity.[5,28,29] However, other limits of integration may be equally valid, particularly in light of the strong overlap of the wings of the $2p_{3/2}$ and $2p_{1/2}$ peaks. In fact, it may be appropriate to subtract off a cosine bell or other double symmetric step function to eliminate the deviation caused by unequal "tailing" of the A^+ and A^- peaks, which may in fact be manifestations of multielectronic effects or dichroic variations of transitions into s and p states, associated with the $L_{\rm III}$ and $L_{\rm II}$ edges. (The position, size, and width, of the cosine bell onset and falloff, or correspondingly the step positions, heights, and widths on peak fitting, are very important, and open to variant interpretation.) Regardless of the method, errors associated with equating $D^+=D^-$, equating $C^+=C^-$, and ascertaining A^+, B^+, A^-, and B^- propagate through the analysis. Thus we return to our assertion that it is difficult to ascertain any of the fractional differences in Eqs. (6)–(8) to better than 0.005, with the resultant errors shown in Table I. A more quantitative and complete description of this process is under preparation.[30]

An intriguing variant of the spectral matching approach is the introduction of the "proportionality" method,[5,28,29] where N is under proportional to the sum:

$$\left[\frac{A^+}{C^+}+\frac{B^+}{C^+}+\frac{A^-}{C^-}+\frac{B^-}{C^-}\right].$$

While this nicely removes the N dependence from Eqs. (7) and (8), it unfortunately removes the very important cancellation of factors between the numerators and denominators of Eqs. (7) and (8). The normalization of the peak areas A^+, B^+, A^-, and B^-now becomes fairly ill defined and the removal of the radial matrix element factor (Appendix A and Refs. 6, 9, and 10) is defeated. Now it is necessary to assume that $(C^{+,-})_i=(C^{+,-})_j$ is an appropriate intersample normalization, implying that the s,p spin-dependent density of states, the p to d radial matrix elements, and the p to s,p transitions are all invariant between different samples or at least vary in such a way to cancel out irregularities. In the original formulation of the sum rules, $C^{+,-}$ is necessary only as a cross-spectral normalization, taking out variations from spectral intensity and sample number (of atoms). Now $C^{+,-}$ becomes an intersample normalization as well, which is far less certain. Despite the admittedly fortuitous agreement of earlier studies[5,28,29,31] it would be wise to approach this method with caution.

Thus we propose a minimum error of $\pm 0.10\mu_B$ for $\mu_{\rm spin}$ and $\pm 0.02\mu_B$ for $\mu_{\rm orb}$ as realistic first-order estimates. Application of these to earlier studies may seri-

TABLE I. Minimum error in magnetic moments. For a 0.005 error in each asymmetry or fractional difference. Using $N=4$ for Fe, $N=3$ for Co, and $N=2$ for Ni; assumes zero error in N.

	Fe	Co	Ni
$\Delta\mu_{\rm spin}^{\rm BR}(\mu_B)$	0.08	0.06	0.04
$\Delta\mu_{\rm spin}^{\rm SR}(\mu_B)$	0.12	0.09	0.06
$\Delta\mu_{\rm orb}^{\rm SR}(\mu_B)$	0.03	0.02	0.013

ously impact the conclusions drawn from them.[4–6,28,29] In our studies, to err on the conservative side, we will use $\pm 0.2\mu_B$ for the spin and $\pm 0.05\mu_B$ for the orbital moments.

IV. EXPERIMENTAL AND SLAB CALCULATION RESULTS

Shown in Table II are the results for Fe/Cu(001). Two cases are considered: low [2 monolayer (ML)] and high (10 ML) coverage. Both are nominally fcc structures, albeit with significant level of disorder[4,32,33] and with a relaxation to bcc at higher coverages.[34] The 10 ML sample with an in-plane magnetization may in fact, suffer from domain closure and alignment effects, causing the small magnetic moment values. The 2 ML sample, with magnetization perpendicular to the surface, exhibits a very large MXCD effect, suggesting dominance of a single domain. Two branching ratio and sum-rule results are included: one using an idealized circular polarization of 100%, and a second, using a realistic 90% circular polarization, reflecting the imperfect characteristics of the beam line. Additionally, we have performed linear muffin-tin orbital (LMTO) calculation (Fig. 4) using a 2 ML Fe/5 ML Cu/2 ML Fe slab, to obtain an independent determination of the spin moment of the 2 ML Fe/Cu(001). All of the observed values of $\mu_{\rm spin}$ fall in the range of 2.0 to 2.5 μ_B, with solid agreement between our slab calculations and the sum-rule result.

Table III contains a summary of results for several Fe/Pt samples of various thicknesses. Again, the ($\mu_{\rm spin}^{\rm BR}$) has two values, one for the idealized 100%, and the other for the realistic 90% polarization.

Consistently, the $\mu_{\rm spin}^{\rm SR}$ and $\mu_{\rm spin}^{\rm BR}$ values agree within the error estimates of $\pm 0.1\mu_B$ or $\pm 0.2\mu_B$. Nevertheless, in the context of our error estimates, one can still observe the trend that $\mu_{\rm spin}^{\rm BR} \le \mu_{\rm spin}^{\rm SR}$ as suggested by Eq. (9). Because $\mu_{\rm spin}^{\rm BR}$ and $\mu_{\rm spin}^{\rm SR}$ are generated from the same fits, some errors will be systematic to both. Nevertheless, there will be some nonsystematic effects, e.g., from the exclusion of the background (C^+, C^-) in the BR calculation and their inclusion in the SR calculation of $\mu_{\rm spin}$. Based upon our error analysis above and the data in Tables II and III, it is possible to make the following observations.

TABLE II. FeCu(001): Fe magnetic moments. See text for details.

		$\mu_{\rm orb}$ (μ_B)	$\mu_{\rm spin}$ (μ_B)
2 ML fcc Fe	Branching ratio (90% pol.)		2.3
	Branching ratio (100% pol.)		2.0
	Sum rules (90% pol.)		2.5
	Sum rules (100% pol.)	0.21	2.3
	Slab calculations	small	2.4
10 ML fcc Fe	Branching ratio (90% pol.)		1.1
	Branching ratio (100% pol.)		1.0
	Sum rules	0.05	1.10

TABLE III. Fe/Pt multilayers: Fe magnetic moments. Layer and interplanar spacings with moment values in μ_B (Fe atom^{-1}). N_l is the number of layer pairs. $t_{\rm Pt}$ is the thickness of the Pt layer. $t_{\rm Fe}$ is the thickness of the Fe layer.

Sample	N_L	$t_{\rm Fe}$	$t_{\rm Pt}$	$\mu_{\rm orb}^{\rm SR}$ (100%)	$\mu_{\rm spin}^{\rm SR}$ (100%)	$\mu_{\rm spin}^{\rm BR}$ (100%)	$\mu_{\rm spin}^{\rm BR}$ (90%)	$\mu_{\rm spin}^{\rm SR}$ (90%)
a	92	0.95	0.95	0.09	0.94	0.85	0.95	1.04
b	100	0.93	0.47	0.08	0.56	0.44	0.49	0.62
c	110	0.53	0.94	0.11	0.27	0.17	0.19	0.30
d	100	0.71	0.93	0.03	0.29	0.24	0.27	0.32
e	75	1.24	0.93	0.12	0.46	0.36	0.40	0.51

(i) At best, $\mu_{\rm orb}^{\rm SR}$ estimates are probably only good to about $\pm 0.05\mu_B$.

(ii) At best, $\mu_{\rm spin}^{\rm SR}$ estimates probably are only good to about $\pm 0.10\mu_B$.

(iii) Using 100% circular polarization, $\mu_{\rm spin}^{\rm BR} \le \mu_{\rm spin}^{\rm SR}$, probably to within about 20% for Fe.

(iv) Branching ratios provide a convenient, easy method to cross-check sum-rule predictions of $\mu_{\rm spin}$, with the constraint that $|\mu_{\rm orb}| \ll |\mu_{\rm spin}|$.

(v) Branching ratios provide a mechanism for proper inclusion of nonideal polarization, i.e., $|P_{h\nu}| < 100\%$. It is reasonable to expect that both $\mu_{\rm spin}^{\rm BR}$ and $\mu_{\rm spin}^{\rm SR}$ should scale the same with $|P_{h\nu}|$, so long as $|\mu_{\rm orb}| \ll |\mu_{\rm spin}|$.

(vi) The branching ratio approach provides easy physical insight into about 80% of the observed behavior in MXCD absorption in 3*d* magnetic materials.

The theoretical calculations of Wu, Wang, and Freeman[21] places similar constraints upon evaluation with the sum-rule analysis. If one accepts the theoretical values of Ref. 21 as being correct, then the limitations or errors discussed by Wu, Wang, and Freeman[21] are actually estimates of the accuracy of the sum-rule method. Our

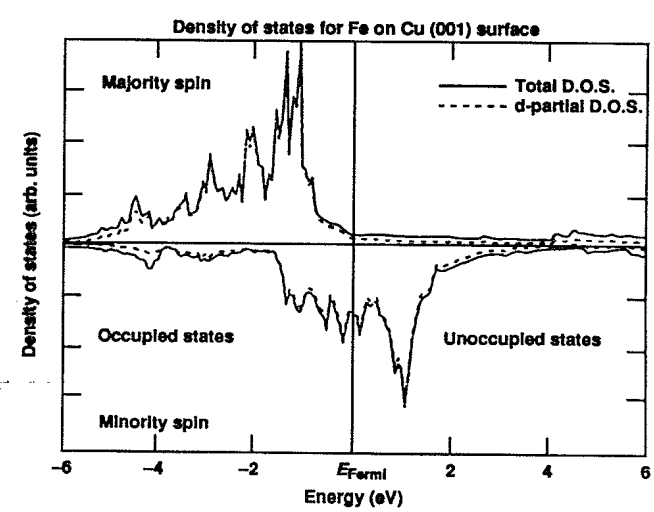

FIG. 4. These are the results of a local density approximation (LDA) slab calculation. The slab consisted of nine layers, 2 Fe/5 Cu/2 Fe. Total density of states (DOS) and *d*-partial DOS are shown, for both the majority and minority spins. Spin-orbit coupling in the valence band has been neglected.

minimum error estimates are more along the lines of precision, e.g., a type of standard deviation. Interestingly, our predictions of limitations in precision for $\mu_{\rm orb}^{\rm SR}$ and $\mu_{\rm spin}^{\rm SR}$ are consistent with the projections of Wu, Wang, and Freeman[21] concerning accuracy. Further work is necessary to ascertain the impact of complications such as band delocalization, multielectronic effects, and noncentrosymmetricity. While the BR analysis provides a quick cross-check of the SR analysis and insight into the physics behind MXCD absorption, the SR analysis is far more complete and well founded. The explicit formulation of the polarization dependence in the BR formula is a useful tool for the experimentalist.

ACKNOWLEDGMENTS

Work performed under the auspices of the U.S. Department of Energy by Lawrence Livermore National Laboratory under Contract No. W-7405-ENG-48. The measurements were performed at the Standard Synchrontron Radiation Laboratory (SSRL), which is supported by the Chemical Sciences Division of the Office of Basic Energy Sciences in the U.S. Department of Energy. Special thanks to Michael Rowen of SSRL and Mahesh Samant, D. Weller, and J. Stohr of IBM, for their work on Beamline 8-2. We also wish to thank Karen Clark . Conversations with P. Carra and T. Thole were enlightening and enjoyable. This work was based upon work supported by the National Science Foundation under Grant No. DMR 94-58004.

APPENDIX A

We have developed a simplified single-electron analysis based upon the ground-breaking original method of Erskine and Sterne,[17] in which a renormalization of raw data is performed to eliminate the nonstatistical contribution and from which the major contributor to $3d$ magnetism, the spin component of the magnetic moment, can be extracted. The justification for this approach is as follows.

(i) The orbital moment contribution to the total moment in $3d$ metals is usually quite small. Consider the results for bulk Fe, Cu, and Ni from Ref. 18. These relativistic calculations predict the ratio of the orbital to spin components ($\mu_{\rm orb}/\mu_{\rm spin}$) to be on the order of 10% or less. Concentrating on the major component is a good first approximation. Moreover, a comparison of these analyses will permit the determination of whether this first operational assumption still holds true. It should be noted that while we are operating in the limit of $\mu_{\rm orb} \ll \mu_{\rm spin}$, a nonzero $\mu_{\rm orb}$ value is absolutely necessary for coupling μ to the lattice.

(ii) The deviation of the linear and circular polarization branching ratios from the statistical values appears to be rooted in many-body effects coupling to the spin-orbit splitting perturbation of the $3d$ valence states.[6,11] As pointed out in Ref. 6, spin-orbit splitting increases $I(2p_{3/2})$ relative to $I(2p_{1/2})$, thus shifting the branching ratios upward, which may be further enhanced by many-body effects such as valence-core hole attraction. Previously, we have proposed that for situations where the deviation of the linear branching ratio from the statistical value of 2/3 is fairly small, that to zeroth order, the nonstatistical effects are the same in BR^+, BR^-, and $\mathrm{BR}^{\rm lin}$. (We will assume throughout that $\mathrm{BR}^+\mathrm{BR}^- = 2\ \mathrm{BR}^{\rm lin}$.) Then, we simply normalized all experimental values by $0.667/\mathrm{Br}_{\rm exp}(\rm lin)$, obtaining the reduced BR′ introduced before.[4] This permitted us to compare the $\mathrm{BR}'_{\rm exp}$ values to the predictions of a simple, one-electron model which has a particularly simple and concise form, shown below. The modified definitions of α and β (previously used in Ref. 4) and $P_{h\nu}$ and P_e are summarized in Table IV),

$$\mathrm{BR}'_{\rm theory} = \frac{3+2(1-\alpha)\beta+2(\alpha)(1-\beta)}{6} = \frac{2}{3} - \frac{1}{6}(P_{h\nu})(P_E)\ . \tag{A1}$$

TABLE IV. Empty valence states/photon helicity. N is the number of empty d valence states. The symbols ↑ and ↓ denote spin-up and spin-down, respectively. α is the spin-down alignment of the d valence states. P_e is the polarization of the d valence states. β is the degree of left circular polarization of the x rays. $P_{h\nu}$ is the circular polarization of the x rays. $F_R(F_L)$ is the intensity flux of the right (left) circularly-polarized component of the x-ray beam.

	Empty valence states		
	Pure down	Pure up	Random
$\alpha = \frac{N^\downarrow}{N^\downarrow+N^\uparrow} = \frac{N^\downarrow}{N}$	1.0	0.0	0.5
$P_e = \frac{N^\downarrow - N^\uparrow}{N^\downarrow+N^\uparrow} = 2\alpha - 1$	1.0	−1.0	0.0
	Photon helicity		
	Positive helicity Pure left circular	Negative helicity Pure right circular	Zero helicity Linear
$\beta = \frac{F_L}{F_R+F_L}$	1.0	0.0	0.5
$P_{h\nu} = \frac{F_L - F_R}{F_R+F_L} = 2\beta - 1$	1.0	−1.0	0.0

[Here, we have restated Eq. (5) to explicitly emphasize the relationship between our new expression and that used previously in Ref. 4.] To derive this expression in a simple-electron picture, a number of additional caveats need to be applied. Perhaps the most important is that concerning the relative unoccupation of the $m_{l=2}$ states. Two possibilities that give rise to Eq. (3) are (a) all $m_{l=2}$'s have equal unoccupation and (b) there is an effective octahedral crystal field splitting. All of this will be discussed below. The key here is that variations of the branching ratio with helicity can be directly related to variations of spin alignment.

Ultimately, it is desirable for it to be possible to go from measured branching ratios directly to elementally-specific magnetic moments. Within the constraints that have been used to derive Eq. (3) and assuming both complete orbital quenching (the Landé g factor being 2, $g=2$) and the validity of atomic configurations, Eq. (6) will be derived. In the next several sections, we will derive the above equations within a single electron picture, discuss the limitations imposed by the assumptions of the derivation, and finally, support our contentions with the results of both modeling and experiments.

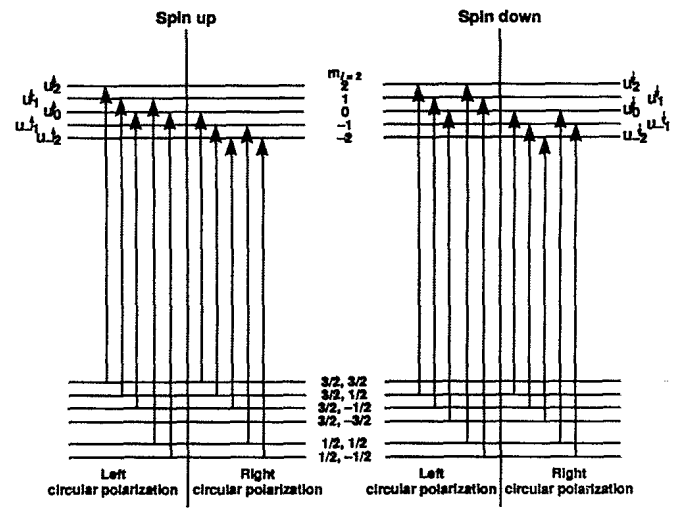

FIG. 5. A schematic of the electric dipole transitions using circular polarization.

Derivations

To obtain Eqs. (A1) and (6), a stepwise sequence will be followed, outlining assumptions and limiting conditions. All of this is based upon circular polarization selection rules, supposing an electric dipole transition between a full p core-level and an empty d valence state [Eqs. (A2) and (A3)]. In this study, the transition could be $3p \rightarrow 3d$ or $2p \rightarrow 3d$. Because of the larger spin-orbit splitting, we will concentrate upon the latter case. This derivation extends the pioneering work of Erskine and Sterne.[17] The reader is also referred to the work by Smith *et al.*,[6] which includes both a number of useful references as well as helpful tables of basis states and matrix elements. As per Jackson,[35] the following are defined:

Left circular polarization–positive helicity

$$\Delta m_l = \Delta m_j = +1, \quad \Delta m_s = 0 \ , \tag{A2}$$

Right circular polarization–negative helicity

$$\Delta m_l = \Delta m_j = -1, \quad \Delta m_s = 0 \ . \tag{A3}$$

Our approach is to consider four boundary cases and then do a weighted sum of the contributions from each case to arrive at a general expression. Each component is dependent upon the size of the spherical harmonic matrix elements and the degree of unoccupation of the final d states. We can take the sum of the four boundary cases because of the particularly fundamental nature of the circular polarization selection rules. The four boundary cases are (a) right circular polarization, spin-up only (empty); (b) right circular polarization, spin-down only (empty); (c) left circular polarization, spin-up only (empty); and (d) left circular polarization, spin-down only (empty) (Fig. 5). We have assumed no j mixing of the initial $P_{3/2}$and $P_{1/2}$ states. Here, a ket notation is used for the initial states and the u's are percentage unoccupied functions. At this point, it is useful to define some matrix elements:

$$\mathcal{A} = \mathcal{A}^{L,R} = |\langle l=2, m_l=\pm 2 | \hat{\partial}^{L,R} | l=1, m_l=\pm 1 \rangle|^2 = (4/5) r \ , \tag{A4}$$

$$\mathcal{B} = \mathcal{B}^{L,R} = |\langle l=2, m_l=\pm 1 | \hat{\partial}^{L,R} | l=1, m_l=0 \rangle|^2 = (2/5) r \ , \tag{A5}$$

$$\mathcal{C} = \mathcal{C}^{L,R} = |\langle l=2, m_l=0 | \hat{\partial}^{L,R} | l=1, m_l=\mp 1 \rangle|^2 = (2/15) r \ . \tag{A6}$$

Here, we have $\hat{\partial}^L$ and $\hat{\partial}^R$ the electric dipole operators, such that $\hat{\partial}^L = q(x+iy)$ and $\hat{\partial}^R = q(x-iy)$, where q is the charge. The symbol r is the radial matrix element factor and includes a number of constants. The magnetic vector $\vec{B}$, and the helicity or polarization vector $\vec{P}_{h\nu}$ are along the z direction, but can independently be parallel or antiparallel with $\hat{z}$. The magnetic vector $\vec{B}$ is meant to generically represent either an applied magnetic field or the remanent magnetization. The helicity or polarization vector, $\vec{P}_{h\nu}$, differentiates between right- and left-handed circular polarization. The key is whether $\vec{B}$ and $\vec{P}_{h\nu}$ are parallel or antiparallel. Because we will deal with the unoccupation functions separately, we can dispense with the separate treatment of the right- and left-handed cases, using simply $\mathcal{A}$, $\mathcal{B}$, and $\mathcal{C}$.

Now, we need to sum the intensity contributions for each boundary case and each initial j state, i.e., $P_{3/2}$ and $P_{1/2}$. For a given spin and circular polarization, there will be two to three terms, each comprised of the radial term, r, times an unoccupation function times an initial m_l state distribution factor times an orbital cross-sectional factor, i.e., $\mathcal{A}$, $\mathcal{B}$, or $\mathcal{C}$.

An example of this would be $I_{3/2}^{L,\uparrow}$, the intensity for the $2p_{3/2}$ peak with left-circular polarization and spin-up only:

$$I_{3/2}^{L,\uparrow}=(r)\left[u_2^{\uparrow}(1)(\mathcal{A})+u_1^{\uparrow}\left[\frac{2}{3}\right]\mathcal{B}+u_0^{\uparrow}\left[\frac{1}{3}\right]\mathcal{C}\right]=(r)\left[\frac{4}{5}u_2^{\uparrow}+\frac{4}{15}u_1^{\uparrow}+\frac{2}{45}u_0^{\uparrow}\right] . \tag{A7}$$

There are eight such equations: two polarizations times two spins times two j states. Next, we take a weighted sum of each contribution, using β and $(1-\beta)$ as the weighting factors for left-handed and right-handed circular polarization. Note that the r's are divided out,

$$\mathrm{BR}_{\mathrm{theory}}=\frac{\beta I_{3/2}^{L,\downarrow}+\beta I_{3/2}^{L,\uparrow}+(1-\beta)I_{3/2}^{R,\downarrow}+(1-\beta)I_{3/2}^{R,\uparrow}}{\beta(I_{3/2}^{L,\downarrow}+I_{1/2}^{L,\downarrow})+\beta(I_{3/2}^{L,\uparrow}+I_{1/2}^{L,\uparrow})+(1-\beta)(I_{3/2}^{R,\downarrow}+I_{1/2}^{R,\downarrow})+(1-\beta)(I_{3/2}^{R,\uparrow}+I_{1/2}^{R,\uparrow})} . \tag{A8}$$

Substituting the expressions such as (A7) into (A8) gives an expression containing sums of polarization factors times unoccupation factors times coefficients. At this point, it is useful to apply some simplifying assumptions, from an extreme situation. Consider the limiting case where all $m_l=2$ states for a given spin are equally unpopulated. Here $u^{\uparrow}=u_i^{\uparrow}$ for $i=-2, -1, 0, 1, 2$, and $u^{\downarrow}=u_i^{\downarrow}$ for $i=-2, -1, 0, 1, 2$,

$$\mathrm{BR}_{\mathrm{theory}}^{\mathrm{eq}}=\frac{\beta\frac{2}{3}u^{\downarrow}+\beta\left[\frac{10}{9}\right]u^{\uparrow}+(1-\beta)\left[\frac{10}{9}\right]u^{\downarrow}+(1-\beta)\left[\frac{2}{3}\right]u^{\downarrow}}{\frac{4}{3}u^{\downarrow}+\frac{4}{3}u^{\uparrow}} . \tag{A9}$$

Now, let us use the definitions of a percentage spin polarization in the empty, unoccupied states, α and also the polarization P_E from Table IV. Under these special conditions we can express P_E, α, and $(1-\alpha)$ in terms of $u^{\uparrow}$ and $u^{\downarrow}$,

$$\alpha=\frac{u^{\downarrow}}{u^{\downarrow}+u^{\uparrow}} , \tag{A10}$$

$$(1-\alpha)=\frac{u^{\uparrow}}{u^{\downarrow}+u^{\uparrow}} , \tag{A11}$$

$$P_E=\frac{u^{\downarrow}-u^{\uparrow}}{u_{\downarrow}+u^{\uparrow}}=2\alpha-1 . \tag{A12}$$

Equation (A9) then becomes the equation (A1) above. So, in the limit that all of the $m_l=2$ states for a given spin are equally unoccupied, Eq. (A1) can be obtained.

It is useful at this point to digress to a consideration of what constitutes the parallel (BR^+) and antiparallel (BR^-) cases of Fig. 3 and Eq. (3). The magnetization and helicity are the quantities called out in Fig. 2. The magnetization will be antiparallel to the majority spin and parallel to the minority. For left-handed or positive helicity radiation that is 100% circularly polarized, $P_{h\nu}=+1$. For this polarization, the parallel (antiparallel) case would have a positive (negative) magnetization, a negative (positive) majority spin, and a positive (negative) minority spin. A positive (negative) minority spin means P_E less (greater) than zero. Thus the parallel (antiparallel) case would have a BR greater (less) than 2/3.

Moreover, we can get the same result if we make a less constricting assumption, an effective octahedral crystal-field splitting (CFS). The general equations for two examples, fcc and bcc metals, are shown below. T and E stand for T_{2g} and E_g symmetry states. There are two major restrictions imposed by the octahedral CFS assumption: (1) the unoccupation functions are dependent upon spin and the absolute value of m ($u_{+m}^{\mathrm{spin}}=u_{-m}^{\mathrm{spin}}$), and (2) $u_{\pm 2}^{\mathrm{spin}}$ equals the average of $u_{\pm 1}^{\mathrm{spin}}$ and u_0^{spin}. (This contains as a subset, $u_{\pm 2}^{\mathrm{spin}}=u_{\pm 1}^{\mathrm{spin}}=u_0^{\mathrm{spin}}$, the first set of conditions above.) If the expressions of Eqs. (A13)–(A17) are inserted into Eq. (A8), once again Eq. (A1) is obtained. However, we now have four independently variable unoccupation factors: $u_T^{\uparrow}$, $u_E^{\uparrow}$, $u_T^{\downarrow}$, and $u_E^{\downarrow}$, with $\alpha=(3u_T^{\downarrow}+2u_E^{\downarrow})/(3u_T^{\downarrow}+2u_E^{\downarrow}+3u_T^{\uparrow}+2u_E^{\uparrow})$,

$$u_2^{\mathrm{spin}}=\frac{1}{2}u_T^{\mathrm{spin}}+\frac{1}{2}u_E^{\mathrm{spin}} , \tag{A13}$$

$$u_1^{\mathrm{spin}}=u_T^{\mathrm{spin}} , \tag{A14}$$

$$u_0^{\mathrm{spin}}=u_E^{\mathrm{spin}} , \tag{A15}$$

$$u_{-1}^{\mathrm{spin}}=u_T^{\mathrm{spin}} , \tag{A16}$$

$$u_{-2}^{\mathrm{spin}}=\frac{1}{2}u_T^{\mathrm{spin}}+\frac{1}{2}u_E^{\mathrm{spin}} . \tag{A17}$$

Finally, it is necessary to invert Eq. (A1) to obtain Eq. (6). Using $\mu_{\mathrm{spin}}/\langle S_z\rangle=2$, Eq. (A18) can be written:

$$\mu_{\mathrm{spin}}^{\mathrm{BR}}=N(2\alpha-1)=N(P_E) . \tag{A18}$$

Inverting Eq. (A1) and substituting into Eq. (A18) gives us the following:

$$\mu_{\mathrm{spin}}^{\mathrm{BR}}=\frac{6(N)}{P_{h\nu}}[\mathrm{BR}'-2/3] . \tag{A19}$$

This is essentially the result used in Ref. 4. Moreover, it is possible to generate a more comprehensive expression by using BR^+ and BR^- for a given $\pm|P_{h\nu}|$. This has the advantage of using both data directly and emphasizing the variation of BR with helicity. The process is shown below, and the normalization of the BR values is shown explicitly.

$$\mu_{\text{spin}}^{\text{BR}}=\frac{\mu_{\text{spin}}^{\text{BR}+}+\mu_{\text{spin}}^{\text{BR}-}}{2}=6(N)\left\{\frac{\left[\frac{(\text{BR}^{+})\left[\frac{2}{3}\right]}{\text{BR}^{+}+\text{BR}^{-}}-\frac{2}{3}\right]}{|P_{h\nu}|}+\frac{\left[\frac{(\text{BR}^{-})\left[\frac{2}{3}\right]}{\text{BR}^{+}+\text{BR}^{-}}-\frac{2}{3}\right]}{-|P_{h\nu}|}\right\}. \tag{A20}$$

Equation (A20) simplifies to Eq. (6). This compact expression, using a branching ratio asymmetry, utilizes the two key pieces of data, BR^{+} and BR^{-}, and directly incorporates the previously discussed normalization for excursions from statisticality, i.e., $(\text{BR}^{+}+\text{BR}^{-})\neq 4/3$. The element-specific spin magnetic moment can be determined solely from N, $|P_{h\nu}|$, BR^{+}, and BR^{-}. In Appendix B, the close relation between this expression and the sum rules will be established. Next the validity of the above approximations will be discussed.

Discussion of limitations and approximations

There are many limitations, approximations, and possible shortcomings to the BR analysis method described so far. Here, there will be discussed, as well as some conceivable solutions and justifications.

The linear branching ratios are not observed experimentally to be the statistical value, 2/3, and it is tempting to adapt the above method to these observations. One possibility is polarization of the $2p$ core levels, that is, mixing of the $2p_{3/2}$ and $2p_{1/2}$ states induced by the magnetic field. We have pursued this and found that to obtain the BR^{lin} value of 0.74 for Fe,[4,11] it would be necessary to change the coefficients of states in Fig. 5 substantially. Basically, the coefficients would go from being $\pm\sqrt{2/3}$ or $\pm\sqrt{1/3}$ to $\pm\sqrt{1/2}$. However, this is physically unreasonable. Experimentally, we have measured the exchange-splitting-induced shift of the $2p^{3/2}-2p^{1/2}$ splitting in 4 ML of Fe/Cu(001).[8] Here, the spin-orbit splitting is on the order of 13 eV and the exchange splitting shift is measured to be 0.33 ± 0.14 eV. (This may be shifted due to peak broadening.) From first-order perturbation theory,[36] the degree of mixing should go as $\Delta E_{\text{ex}}/\Delta E_{\text{spin orbit}}$. The experimental value is $(0.33\pm0.14\ \text{eV})/13\ \text{eV}=2.5\%\pm1\%$. To achieve the observed BR^{lin} values of 0.74 eV would require mixing of about 17%, which is much greater than the experimental value. While this is a gross oversimplification of the issue of core exchange shifts[37] it seems unlikely that core polarization is playing a dominant role here.

It should also be pointed out that, strictly speaking, the radial factors for the unpolarized $2p^{3/2}$ and $2p^{1/2}$ states are not identical. While the nonrelativistic R_{nd} are equivalent, the relativistic R_{nj} can be different. From our slab calculations discussed below, we can estimate the impact upon the radial matrix elements of the two transition types. The variation is less than 1%, consistent with earlier observations,[6,9] which is negligible under these conditions.

More importantly, we should consider the assumptions of (1) all u_{ml}^{spin} being equal, for a given spin, and (2) the effective octahedral crystal-field-splitting case. Two sets of conditions could give rise to all of the u_{ml} for a given spin being equal: (a) an atomic situation with all of the $3d$ states degenerate, ignoring the small spin-orbit splitting of the valence $3d$ states [$\xi(\text{Fe})=0.05$ eV and $\xi(\text{Ni})=0.1$ eV, from Ref. 6]; (b) complete mixing induced by effects such as large dispersion. Both of these are fairly unlikely, although they could be good staring points. More physically appealing is the second case, as effective octahedral crystal-field splitting within a larger exchange splitting. For our approximation to work the dominant potential terms must be the exchange splitting and effective crystal-field splitting, followed by the perturbations associated with dispersion, spin-orbit splitting, and Zeeman splitting of the m_l states. For example, if the spin-orbit splitting would become too large relative to the exchange splitting, the decoupling of the spin-up manifold from the spin-down manifold would fail. However, consider the supercell calculation result 2 Fe/5 Cu/2 Fe shown in Fig. 4. This supercell calculation does not include spin-orbit splitting in the valence bands but it does compare well with more relativistic overlayer calculations[38] and its predictions of magnetic moments agrees nicely with the relativistic calculations[18] introduced earlier. The important point here is that the exchange splitting can be seen to be about 2 eV: thus the ratio of $\Delta E_{\text{S.O.}}/\Delta E_{\text{ex}}\approx 0.05\ \text{eV}/2\ \text{eV}=2.5\%$, using the spin-orbit splitting parameter, $\xi=0.05$ eV, from Ref. 6. Clearly, the exchange splitting dominates the spin-orbit splitting.

A similar condition is necessary in terms of an effective crystal-field splitting versus band dispersion. Obviously, in metallic systems the valence and conduction bands are dispersive, the energy of each state depending in part upon its position in k space. This contributes to the finite bandwidth observed in density of states calculations, an example of which is shown in Fig. 4. However, in absorption measurements, momentum is not resolved and it may be more appropriate to frame our analysis in terms of density of states that reflects effective crystal potential. In our derivation of branching ratio relations, it was found that a dominant octahedral crystal-field splitting was consistent with Eq. (A1). But the question remains: will the dispersive effects coupled with momentum conservation in each individual transition be sufficient to impose the space-group symmetry as a dominant potential or will the averaging over the zone be complete enough to induce an effective crystal-field splitting with the point-group symmetry of the Γ point of the Brillouin zone? The crux of the issue is whether the relation $u_{\pm2}^{\text{spin}}=\frac{1}{2}u_{\pm1}^{\text{spin}}+\frac{1}{2}u_{0}^{\text{spin}}$ actually holds. To address this question, the majority and minority density of states of bulk bcc Fe and fcc Ni have been decomposed into their

E_g and T_{2g} components. An example is shown in Fig. 6. The above relation is found true to typically within about 10%. In retrospect, this result is not surprising.[39] Additionally, it is also possible to use these results to confirm the expectation of strong orbital quenching:[24] the effective crystal field energies are on the order of volts, whereas $\xi \approx 0.1$ eV (Ref. 6).

Related to this issue is the possibility of a Zeeman splitting perturbation of the m_l and $-m_l$ states. From the derivation above, it is obvious that if all the u_{ml}^{spin} are independent, almost any BR can be obtained. Again the strongest argument against the lifting of the $\pm m_l$ degeneracy is the retention of strong octahedral crystal-field splitting, described above. Effective crystal-field splitting such as this provides for quenching of the orbital contribution (whether spin-orbit or Zeeman-induced) to the magnetic moment. Thus the octahedral splitting approximation seems to hold to within about 15% or less, for the worst case system of a metal. It seems likely that it will work even better with metallic oxides and other localized systems.

A further approximation used here is the neglect of the s electron density of states in the unoccupied states. The core p electron can undergo dipolar transitions to a d electron state, as assumed here, but p to s transitions are also allowed. These transitions will be negligible if the s final state density is much smaller than the d final state density. If this is not the case, the matrix elements take the form $|\langle \text{initial}p|V|\text{final}s+d\rangle|\text{^}2$, which leads to the obvious terms $|\langle \text{initial}p|V|\text{final}d\rangle|\text{^}2$, $|\langle \text{initial}p|V|\text{final}s\rangle|\text{^}2$, and the cross term or interference term, $\langle \text{initial}p|V|\text{final}d\rangle\langle \text{final}s|V|\text{initial}p\rangle$. Both the s contribution and the interference term are ignored in this analysis, and their inclusion provides yet another means of changing the linear branching ratio from its statistical value.[20]

Finally, a very important assumption in our analysis is that the valence states are either pure spin-up or spin-down. This is a valid assumption provided spin-orbit coupling is small, as is the case for the $3d$ transition metals, but is not true for the $4f$ elements. If spin-orbit effects were not negligible, one consequence would be to introduce interference effects between the spin-up and spin-down final states for all the $m_j=1/2$ states. The $m_j=\pm 3/2$ are not affected since they only couple to one spin component for a given polarization. An alternative procedure would be to treat the valence states in an m_j representation, which is a more natural one for atomic-like orbitals.

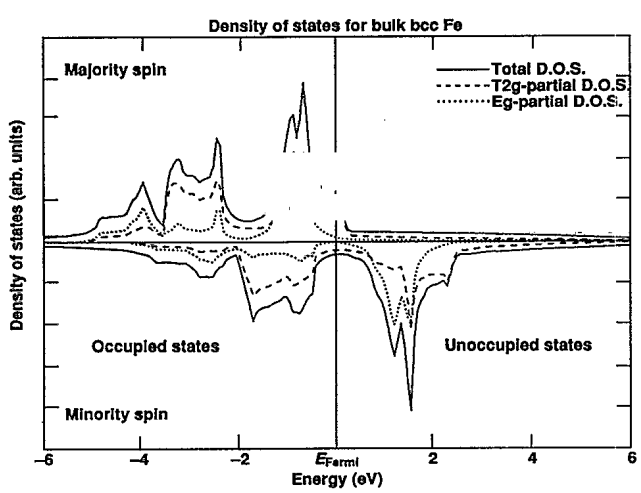

FIG. 6. A spin-polarized LDA calculation for bulk bcc Fe, including a decomposition into $t2g$ and eg density of states.

APPENDIX B

Recently, Carra *et al.*[10] derived a sum rule for electric dipole transitions in a single ion model that could be used to extract an elementally-specific spin magnetic moment (μ_{spin}) from magnetic x-ray circular dichroism spectra. Earlier, we proposed the utilization of a branching ratio analysis[4] of the determination of μ_{spin}, based upon a simplified one-electron, atomic picture which assumed complete orbital quenching. Here, it will be shown that these two approaches are essentially equivalent in the case of $3d$ ferromagnetic materials. Both methods are based upon a comparison of the integrated intensity in the $L_{\text{III}}(J=3/2)$ white line peak versus the sum of the intensities in the $J=3/2$ and $L_{\text{II}}(J=1/2)$ peaks, after background removal. An error estimate will also be presented.

Consider Eqs. (B1) and (B2), taken from Ref. 10,

$$\rho=\frac{\int_{j^++j^-}d\omega(\mu^+-\mu^-)}{\int_{j^++j^-}d\omega(\mu^++\mu^++\mu^0)}=\frac{1}{2}\frac{l(l+1)+2-c(c+1)}{l(l+1)(4l+2-n)}\langle L_z\rangle\ , \tag{B1}$$

$$\delta=\frac{l(l+1)-2-c(c+1)}{3c(4l+2-n)}\langle S_z\rangle+A(c,l,m)\langle T_z\rangle=\frac{\int_{j^+}d\omega(\mu^+-\mu^-)-\frac{c+1}{c}\int_{j^-}d\omega(\mu^+-\mu^-)}{\int_{j^++j^-}d\omega(\mu^++\mu^-+\mu^0)}\ . \tag{B2}$$

For the case of $3d$ magnetic materials and using the $2p\rightarrow 3d$ transition, $c=1$ and $l=2$. The number of $3d$ electrons (holes) is $n(10-n)$. In our notation,

$$I_{3/2}^+=\int_{j^+}d\omega\,\mu^+,\quad I_{3/2}^-=\int_{j^+}d\omega\,\mu^-\ ,$$
$$I_{1/2}^+=\int_{j^-}d\omega\,\mu^+,\quad I_{1/2}^-=\int_{j^-}d\omega\,\mu^-\ .$$

Switching to our notation and using $\mu^0=1/2(\mu^++\mu^-)$ as in Ref. 10, a combination and rearrangement of Eqs. (B1) and (B2) gives us Eq. (B3), shown below:

$$2\langle S_z\rangle+3\langle L_z\rangle=6(10-n)\frac{[I_{3/2}^+-I_{3/2}^-]}{[I_{3/2}^++I_{1/2}^++I_{3/2}^-+I_{1/2}^-]}\ . \tag{B3}$$

Here we have also taken the liberty of dropping $\langle T_z\rangle$ as done previously in Ref. 10. Again, Eq. (B3) is merely a restatement of the sum rules of Carra *et al.* using our notation and explicitly showing the spin moment

($\mu_{\rm spin}^{\rm SR}=2\langle S_z\rangle$) and orbital moment ($\mu_{\rm orb}^{\rm SR}=\langle L_z\rangle$). The superscript SR stands for sum rule.

Now consider the branching ratio analysis previously proposed in Ref. 4 [see Eqs. (A1), (A19), and (A20). Here, we use $\mathrm{BR}^{+}+\mathrm{BR}^{-}=2\,\mathrm{BR}^{\rm lin}$. Again, lin +, and − denote polarization: linear, parallel, and antiparallel (helicity and magnetization]. $P_{h\nu}$ is the circular polarization (+1 for left; 0 for linear, and −1 for right circular). For the remainder of this work, $|P_{h\nu}|=1$, to be consistent with Carra *et al.* By doing a series expansion of Eq. (6) and rearranging, we can get Eq. (B4). (This requires dropping terms of 1% magnitude or smaller)

$$\mu_{\rm spin}^{\rm BR}=\frac{4(10-n)}{a}\frac{[I_{3/2}^{+}-I_{3/2}^{-}]}{[I_{3/2}^{+}+I_{1/2}^{+}+I_{3/2}^{-}+I_{1/2}^{-}]}-3\langle L_z\rangle\ ; \tag{B4}$$

here

$$a=\left[\frac{I_{3/2}^{+}+I_{3/2}^{-}}{I_{3/2}^{+}+I_{1/2}^{+}+I_{3/2}^{-}+I_{1/2}^{-}}\right]$$
$$\cong\frac{1}{2}(\mathrm{BR}^{+}+\mathrm{BR}^{-})\cong\mathrm{BR}^{\rm lin}\ , \tag{B5}$$

thus

$$\mu_{\rm spin}^{\rm BR}-\mu_{\rm spin}^{\rm SR}=\left[6-\frac{4}{a}\right](10-n)\left[\frac{I_{3/2}^{+}-I_{3/2}^{-}}{I_{3/2}^{+}+I_{1/2}^{+}+I_{3/2}^{-}-I_{1/2}^{-}}\right]. \tag{B6}$$

In a single electron picture with complete orbital quenching and a statistical branching ratio for linear polarization ($\mathrm{BR}^{\rm lin}=2/3$), $a=2/3$, and $\mu_{\rm spin}^{\rm SR}=\mu_{\rm spin}^{\rm BR}$. Now, it is well known[6,11] that $\mathrm{BR}^{\rm lin}\neq 2/3$, with the causes including $\langle L_z\rangle\neq 0$, band dispersion and multielectronic effects.[6]

However, for the 3*d* magnetic materials, $\langle L_z\rangle/\langle S_z\rangle$ is often quite small[1−3] and the $\mathrm{BR}^{\rm lin}$ value and a are close to 2/3. The derivation of a from 2/3 is a measure of the error. To be more specific, we can apply Eq. (B7),

$$\%\ \text{error}=\left|\frac{\mu_{\rm spin}^{\rm SR}-\mu_{\rm spin}^{\rm BR}}{\mu_{\rm spin}^{\rm SR}}\right|\cong\left|\left[\frac{a-2/3}{a}\right]\left[1+\frac{3\langle L_z\rangle}{2\langle S_z\rangle}\right]\right|. \tag{B7}$$

Using the values from Ref. 10, $1+3\langle L_z\rangle/2\langle S_z\rangle\leq 1.25$. As an example, consider Fe/Cu(001), where $a\cong 0.73$ and $\langle L_z\rangle/\langle S_z\rangle=0.1$: here the % error would be 10%. For Ni and Co the error would probably be higher: to be conservative, a value of 20% can be used as a rule of thumb.

Thus the approximate analysis procedure using branching ratios, based upon on atomic, single-electron picture and assuming strong orbital quenching, can give the same value of $\mu_{\rm spin}$ as the sum-rule approach, to within 20% or better. This can be done without explicit knowledge of $\langle L_z\rangle$ and without cross normalization between spectra. Finally, it is necessary to note that both of these models are grounded in localized atomic or ionic pictures. Band dispersion and multielectronic effects ultimately must be included for full analysis.[6]

[1]G. Shütz, W. Wagner, W. Wilhelm, P. Keinle, R. Zeller, R. Frahm, and G. Materlike, Phys. Rev. Lett. **58**, 737 (1987).

[2]G. Shütz, R. Frahm, P. Mautner, R. Wienke, W. Wagner, W. Wilhelm, and P. Kienle, Phys. Rev. Lett. **62**, 2620 (1989).

[3]C. T. Chen, F. Sette, Y. Ma, and S. Modesti, Phys. Rev. B **42**, 7262 (1990).

[4]J. G. Tobin, G. D. Waddill, and D. P. Pappas, Phys. Rev. Lett. **68**, 3642 (1992); G. D. Waddill, J. G. Tobin, and D. P. Pappas, J. Appl. Phys. **73**, 6748 (1993).

[5]Y. Wu, J. Stohr, B. D. Hermsmeier, M. G. Samant, and D. Weller, Phys. Rev. Lett. **69**, 2307 (1992); M. G. Samant, J. Stohr, S. S. P. Parkin, G. A. Held, B. D. Hermsmeier, F. Herman, M. Van Schilfgaarde, L. C. Duda, D. C. Mancini, N. Wassdahl, and R. Nakavima, Phys. Rev. Lett. **72**, 1112 (1994).

[6]N. V. Smith, C. T. Chen, F. Sette, and L. F. Mattheiss, Phys. Rev. B **46**, 1023 (1992); C. T. Chen, N. V. Smith, and F. Sette, *ibid.* **43**, 6785 (1991).

[7]L. Baumgarten, C. M. Schneider, M. Petersen, F. Schafers, and J. Kirschner, Phys. Rev. Lett. **65**, 492 (1990).

[8]G. D. Waddill, J. G. Tobin, and D. P. Pappas, Phys. Rev. B **46**, 552 (1992).

[9]B. T. Thole, P. Carra, F. Sette, and G. Van der Laan, Phys. Rev. Lett. **68**, 1943 (1992).

[10]P. Carra, B. T. Thole, M. Altarelli, and X. Wang, Phys. Rev. Lett. **70**, 694 (1993); P. Carra, Synth. Rad. News. **5**, 21 (1992); P. Carra (unpublished).

[11]B. T. Thole and G. Van der Llan, Phys. Rev. B **38**, 3158 (1988); Phys. Rev. A **38**, 1943 (1992); G. Van der Laan and B. T. Thole, Phys. Rev. B **42**, 6670 (1990); **43**, 13 401 (1991).

[12]A. F. Jankowski, G. D. Waddill, and J. G. Tobin, J. Vac. Sci. Tecnol. A **12**, 2215 (1994).

[13]J. G. Tobin and G. D. Waddill, Mod. Phys. Lett. B **7**, 317 (1993).

[14]A. Nilson, J. Stohr, T. Wiell, M. Alden, P. Bennich, D. Wass Dahl, B. Johansson, J. Nordgren, and N. Martensson (unpublished).

[15]A. F. Starace, Phys. Rev. B **5**, 1773 (1972).

[16]E. O. F. Zdansky, A. Nilsson, J. Tillborg, O. Bjorneholm, N. Martensson, J. N. Andersen, and R. Nyhom, Phys. Rev. B **48**, 2632 (1993).

[17]J. L. Erskine and E. A. Stern, Phys. Rev. B **12**, 5016 (1975).

[18]D. Eriksson, B. Johanson, R. C. Albers, A. M. Boring, and M. S. S. Brooks, Phys. Rev. B **42**, 2707 (1990).

[19]Extensive earlier studies (Refs. 6 and 11) have unequivocally demonstrated that a single electron picture without the inclusion of conduction-band spin-orbit splitting fails to predict the experimentally-observed results. In a simple, single-electron picture, without spin-orbit splitting in the valence states the ratio of $I(3/2)/I(3/2)$ should be simply 4/2 or 2.

This gives rise to an expected statistical BR^{lin} of 4/(4+2) or 2/3. However, this is not observed. While inclusion of relativistic effects (spin-orbit splitting) in the metallic valence bands can produce a deviation from the statistical ratio, an unphysically large splitting parameter is necessary for quantitative agreement (Ref. 6). Thole and van der Laan (Ref. 11) have been able to explain these nonstatistical BR^{lin} values in atomic and localized states by resorting to a many-body picture utilizing a Slater-integral approach and spin-orbit splitting, ultimately extending their analysis to magnetic dichroism. Ideally, proper analysis would thus include relativistic effects in the conduction bands, a many-body formalization, and a capacity of dealing with band dispersion (i.e., electron delocalization).

[20]C. T. Chen, Y. U. Idzerda, H. J. Lin, G. Meigs, and N. V. Smith, J. Appl. Phys. **75**, 6378 (1994).

[21]R. Wu, D. Wang, and A. J. Freeman, Phys. Rev. Lett. **71**, 3581 (1993); J. Appl. Phys. **75**, 5802 (1994).

[22]W. L. O'Brien, B. P. Tonner, G. R. Harp, and S. S. P. Parkin, J. Appl. Phys. **76**, 6462 (1994).

[23]C. Kittel, *Introduction to Solid State Physics* (Wiley, New York, 1976), p. 144.

[24]K. G. Tirsell and J. Karpenko, Nucl. Instrum. Methods A **291**, 511 (1990).

[25]L. J. Terminello, G. D. Waddill, and J. G. Tobin, Nucl. Instrum. Methods A **319**, 271 (1992).

[26]J. G. Tobin, G. D. Waddill, Hua Li, and S. Y. Tong, in *Atomic Scale Imaging of Surfaces and Interfaces,* edited by D. K. Biegelson, D. J. Smith, and D. S. Y. Tong, MRS Symposia Proceedings No. 295 (Materials Research Society, Pittsburgh, 1993), p. 213.

[27]J. G. Tobin, M. K.Wagner, X. Q. Guo, and S. Y. Tong, in *Advances in Surface and Thin Film Diffraction,* edited by T. C. Huang, P. J. Cohen, and D. J. Eaglesham, MRS Symposia Proceedings No. 208 (Materials Research Society, Pittsburgh, 1991), p. 283.

[28]J. Stohr and Y. Wu, *New Directions in Research with 3rd Generation Soft X-Ray Synchrontron Radiation Sources* (Kluwer, Netherlands, 1993).

[29]D. Weller, Y. Wu, J. Stohr, M. G. Samant, B. D. Hermsmeier, and C. Chappert, Phys. Rev. B **49**, 12 888 (1994).

[30]P. J. Bedrossian, J. G. Tobin, and G. D. Waddill (unpublished). For a parallel example of spectral matching with photoemission spectra, see G. D. Waddill, J. G. Tobin, X. Guo, and S. Y. Tong, Phys. Rev. B **50**, 6774 (1994).

[31]Using the peak areas of Table III in Ref. 29, it is possible to get a set of values for μ_{orb} which show much the same trends versus the theory, particularly when applying the proffered error of $\pm 0.04\mu_B$.

[32]D. D. Chambliss, R. J. Wilson, and S. Chiang, J. Vac. Sci. Technol. A **10**, 1993 (1992).

[33]D. A. Fowler, M. W. Hart, and J. Barth (unpublished).

[34]S. A. Chambers *et al.*, Phys. Rev. B **36**, 8992 (1987).

[35]J. D. Jackson, *Classical Electro-Dynamics,* 2nd ed. (Wiley, New York 1975), pp. 274–275.

[36]E. E. Anderson, *Modern Physics and Quantum Mechanics* (W. B. Saunders Co., Philadelphia, 1971).

[37]E. Tamura, G. D. Waddill, J. G. Tobin, and P. A. Sterne, Phys. Rev. Lett. **73**, 1533 (1994).

[38]C. L. Fu and A. J. Freeman, Phys. Rev. B **35**, 925 (1987).

[39]In cubic systems, it is convenient to write the wave functions in terms of the *eg* and *t2g* components, which provide a complete set of basis functions for the angular part of the *d*-electron wave function on each atom (von der Lage and Bethe, 1947). By construction, the *eg* and *t2g* components do not mix under the application of the cubic symmetry operations. We can therefore decompose the *d* component of the electron wave function into an *eg* and *t2g* part which we invariant under the cubic symmetry operations (Cornwell, 1969). Since the wave function at each *k* point has a well-defined *eg* and *t2g* component, the density of states corresponding to the *d* electrons can also be decomposed into *eg* and *t2g* terms. This representation is particularly useful when considering the density of states (DOS) corresponding to each of the m_1 components of the *d*-state density. For example, the $m_\{1-0\}$ component is just half the *eg* component, $m_\{1\neq 0\}=1/2$ DOS(*eg*), $m_\{1=1\}=1/3$ DOS(*t2g*) and $m_\{1=2\}=1/4$ DOS(*eg*)+1/6 DOS(*t2g*). A decomposition into *eg* and *t2g* therefore provides the state densities associated with each of the m_1 components without the need for further decomposition (von der Lage and Bethe, 1947). F. C. von der Lage and H. A. Bethe, Phys. Rev. **71**, 612 (1974); J. F. Cornwell, *Group Theory and Electronic Energy Bands in Solids* (Wiley, New York, 1969).